Segregation and temperature effect on the atomic structure of $Bi_{30}Ga_{70}$ liquid alloy

2009 J. Phys.: Condens. Matter 21 245107

(http://iopscience.iop.org/0953-8984/21/24/245107)

J. Phys.: Condens. Matter **21** (2009) 245107 (6pp) doi:10.1088/0953-8984/21/24/245107

Segregation and temperature effect on the atomic structure of $Bi_{30}Ga_{70}$ liquid alloy

D Es Sbihi[1], B Grosdidier[1], I Kaban[2], S Gruner[2], W Hoyer[2] and J-G Gasser[1]

[1] Laboratoire de Physique des Milieux Denses, Institut de Chimie Physique et Matériaux, Université Paul Verlaine—Metz, 1 Boulevard Arago 57078 Metz Cedex 3, France
[2] Institute of Physics, Chemnitz University of Technology, D-09107 Chemnitz, Germany

E-mail: grosdidi@univ-metz.fr

Received 24 February 2009, in final form 6 April 2009
Published 21 May 2009
Online at stacks.iop.org/JPhysCM/21/245107

Abstract

We investigate the structure of liquid monotectic alloy $Bi_{30}Ga_{70}$ above and below the critical point. The three-dimensional structure at 265 °C is modelled by means of the reverse Monte Carlo simulation technique using neutron and x-ray diffraction experimental data. It is shown that atomic segregation on the short-range scale exists in the liquid $Bi_{30}Ga_{70}$ slightly above the critical temperature ($T_C = 262$ °C). We present also the structure factors of $Bi_{30}Ga_{70}$ liquid alloy under the critical point at 240 and 230 °C obtained with neutron diffraction to highlight the temperature effect in the atomic structure.

(Some figures in this article are in colour only in the electronic version)

1. Introduction

The study of segregation in liquid alloys (so-called monotectic alloys) has always been a subject of interest for physicists [1]. It is interesting to study the correlation between the local structure, thermodynamic [2] and electrical transport properties [3]. It is known that the temperature dependences of different physical properties exhibit a specific behaviour by approaching the critical temperature T_C. The dynamic viscosity significantly deviates from the Arrhenius type of behaviour in a temperature range of some kelvins above T_C as has been shown, for example, for a liquid Bi–Ga system by Vollmann and Riedel [4]. The small-angle diffraction experiments with monotectic alloys revealed a remarkable increase of the scattered intensity upon decreasing alloy temperature down to the critical point [5, 6]. These phenomena are related to the concentration fluctuations in the monotectic alloys near T_C.

Bhatia and Thornton [7] related the concentration–concentration structure factor at the low scattering angle limit with the Gibbs energy of the alloy and showed that the structure factor at zero scattering angle becomes infinity by demixing. Hoshino and Young [8] established that in the case of segregation in the binary alloy the maxima of the homonuclear partial pair correlation functions $g_{11}(r)$ and $g_{22}(r)$ are higher than the maximum of the heteronuclear pair correlation function $g_{12}(r)$.

The Bi–Ga system is characterized by a liquid–liquid miscibility gap ranging from 38.5 to 91.5 at.% Ga at the monotectic temperature $T_M = 222$ °C [9]. The critical point is located at about 70 at.% Ga and the critical temperature is $T_C = 262$ °C.

Saito *et al* [10] studied liquid $Bi_{30}Ga_{70}$ alloys at 317 °C with the anomalous x-ray scattering method and determined partial structure factors. They found that the partial structure function for Bi–Bi pairs differs from the pure Bi case, while the partial structure function for Ga–Ga pairs was rather similar to that of pure Ga. In this paper we present a study of $Bi_{30}Ga_{70}$ liquid alloy using experimental neutron diffraction (ND) and x-ray diffraction (XRD) experiments and the reverse Monte Carlo (RMC) modelling technique, which enables us to obtain the three partial pair distribution functions and partial structure factors. These results are used to interpret the structure of the $Bi_{30}Ga_{70}$ liquid alloy above and below the demixing temperature. In reciprocal space, segregation in the sense of preferred homo-coordination becomes apparent as clearly shown by the Bhatia–Thornton partial functions and the Cargill–Spaepen short-range order parameter [11]. In real space, segregation is revealed by the Hoshino–Young criterion.

In section 2 we firstly recall the relations between the structure factor $a(q)$ and the pair correlation function $g(r)$ and

we give the criterion of segregation based on these quantities. In section 3 we recall the neutron and x-ray experimental setup, and our results are presented and discussed in section 4. Finally, a short conclusion is given.

2. Theoretical tools

2.1. Structure factors—pair correlation functions—segregation

In the Faber–Ziman (FZ) formalism [12, 13], the total structure factor $a^{\mathrm{FZ}}(q)$ of a binary alloy is related to the partial structure factors $a_{ij}(q)$ by the relationship:

$$a^{\mathrm{FZ}}(q) = w_{11}^{K} a_{11}(q) + 2w_{12}^{K} a_{12}(q) + w_{22}^{K} a_{22}(q). \quad (1)$$

Here q denotes the magnitude of the scattering vector $q = 4\pi \sin\Theta/\lambda$, where Θ is half the scattering angle and λ is the wavelength used in the scattering experiment. The weights w_{ij}^{K} in formula (1) are equal to:

$$w_{ij}^{\mathrm{N}} = \frac{c_i c_j b_i b_j}{(c_1 b_1 + c_2 b_2)^2} \quad \text{for neutron scattering,} \quad (2a)$$

and

$$w_{ij}^{\mathrm{X}}(q) = \frac{c_i c_j f_i(q) f_j(q)}{(c_1 f_1(q) + c_2 f_2(q))^2} \quad \text{for x-ray scattering,}$$
respectively. (2b)

In the formulae (2) c_i, b_i and $f_i(q)$ are the concentration, the neutron scattering length ($b_{\mathrm{Bi}} = 8.533$ fm and $b_{\mathrm{Ga}} = 7.29$ fm [14]) and the q-dependent x-ray form factor ($f_{\mathrm{Bi}}(q = 0) = 83$ e.u. and $f_{\mathrm{Ga}}(q = 0) = 31$ e.u.) of the pure metal i, respectively.

The Faber–Ziman partial structure factors $a_{ij}(q)$ are linked to the partial pair correlation functions $g_{ij}(r)$ by:

$$g_{ij}(r) - 1 = \frac{1}{2\pi^2 \rho_0 r} \int_0^\infty q(a_{ij}(q) - 1) \sin(qr)\, \mathrm{d}q, \quad (3)$$

or

$$a_{ij}(r) - 1 = \frac{4\pi\rho_0}{q} \int_0^\infty r(g_{ij}(r) - 1) \sin(qr)\, \mathrm{d}r, \quad (4)$$

where ρ_0 is the average number density of the alloy.

In the Bhatia–Thornton formalism [7], the concentration–concentration correlation structure factor $S_{\mathrm{CC}}(q)$ is an indicator of the chemical order and is related to the FZ partial structure factors by:

$$S_{\mathrm{CC}}(q) = c_1 c_2 (1 + c_1 c_2 (a_{11}(q) + a_{22}(q) - 2a_{12}(q))). \quad (5)$$

Segregation in an alloy is displayed in increasing $S_{\mathrm{CC}}(q)$ at low q values. Ruppersberg and Knoll [15] investigated the phase separation in liquid Li–Na alloy experimentally by neutron scattering and showed that $S_{\mathrm{CC}}(0) \to \infty$ on the spinodal curve.

The segregation is manifested also on the Faber–Ziman partial structure factors $a_{11}(q)$ and $a_{22}(q)$ which tend to plus infinity at $q = 0$ and the partial structure factor $a_{12}(q)$ which tends to minus infinity at $q = 0$. The expressions of the terms $a_{11}(q = 0)$, $a_{22}(q = 0)$ and $a_{12}(q = 0)$ are given by Singh and Sommer [1].

The Fourier transform of $S_{\mathrm{CC}}(q)/(c_1 c_2)$ is given by:

$$\frac{1}{2\pi^2 \rho_0 r c_1 c_2} \int_0^\infty q \left(\frac{S_{\mathrm{CC}}(q)}{c_1 c_2} - 1 \right) \sin(qr)\, \mathrm{d}q = g_{11}(r) + g_{22}(r) - 2g_{12}(r). \quad (6)$$

The quantity $g_{11}(r)+g_{22}(r)-2g_{12}(r)$ is linked to the difference between the homo-coordination characterized by $g_{11}(r) + g_{22}(r)$ and the hetero-coordination characterized by $2g_{12}(r)$ and indicates the nature of the chemical order in the first nearest neighbours shell.

Details describing the technique of RMC modelling can be found in [16, 17]. The reliability of the modelled partial pair distribution functions and structure factors is high if the modelling is performed on at least two independent scattering experiments showing enough contrast [18, 19].

3. Experiments

3.1. Neutron scattering

The ND measurements have been performed with the 7C2 diffractometer at the LLB (CEA Saclay, France) described in detail in [20]. The neutron beam section is equal to 5×2 cm^2. The magnitude of the scattering vector is in the range from 0.3 to 16 Å^{-1}, the experimental wavelength $\lambda = 0.709$ Å. The angular resolution and the number of detector cells are equal to 0.2° and 640, respectively. The highest neutron flux value is approximately 2×10^7 neutrons cm^{-2} s^{-1} at the wavelength used.

The $Bi_{30}Ga_{70}$ alloy was prepared from Bi and Ga of purity 99.999%. The sample is put in the amorphous silica cell, which is placed in a special turning device inside the vacuum furnace that allows the homogenization of the liquid alloy. Furthermore, the vertically moving window placed on the neutron beam permits measurement of the liquid alloy structure in different parts of the sample, i.e. separate investigation of the two demixed liquid phases when the temperature is decreased below T_{C}.

The corrections of the scattering intensity for background, furnace, empty container effects, self-absorption, multiple scattering, inelastic scattering and incoherent scattering contributions are done following the procedures described elsewhere [21]. The quality of these corrections is estimated by using a vanadium rod, which presents the same geometric characteristics as the sample, namely a cylinder with a height of 60 mm and diameter of 8 mm.

3.2. X-ray scattering

The XRD measurements have been performed with the Θ–Θ high-temperature diffractometer at Chemnitz University of Technology (Chemnitz, Germany) described in [22]. The alloy is placed in a crucible of internal dimensions equal to 24 mm × 39 mm × 2 mm. The sample temperature is measured by a NiCr–Ni-thermocouple inserted into the crucible bottom. The temperature is kept constant within ±1 K of the set point during the experiment. Before heating, the chamber with

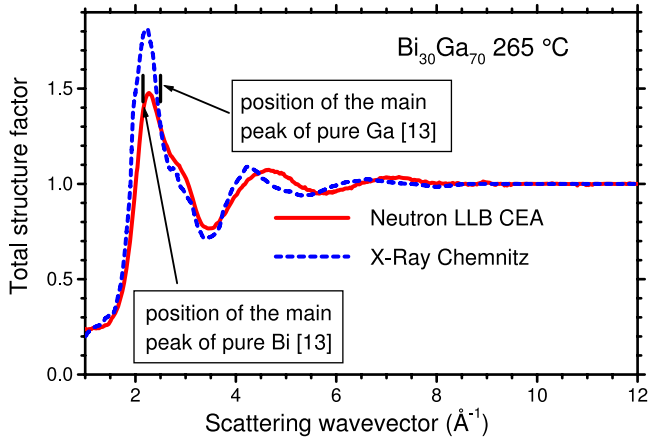

Figure 1. Total structure factors $a^{\mathrm{Exp-N}}(q)$ and $a^{\mathrm{Exp-X}}(q)$ obtained from neutron scattering (*full line*) and from x-ray diffraction (*dashed line*) for the $Bi_{30}Ga_{70}$ liquid alloy at 265 °C, respectively.

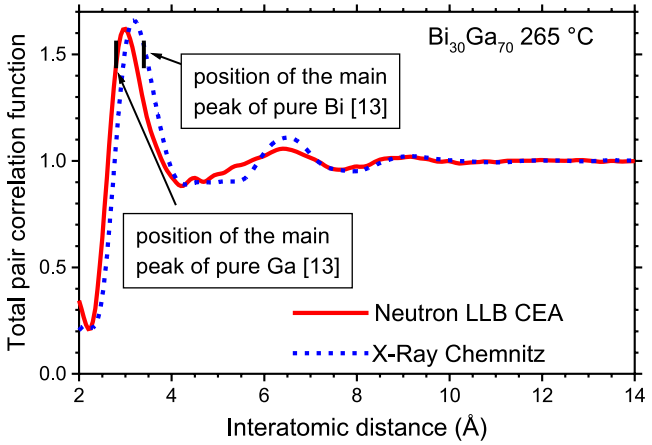

Figure 2. Experimental pair correlation functions $g^{\mathrm{Exp-N}}(r)$ (*full line*) and $g^{\mathrm{Exp-X}}(r)$ (*dashed line*) obtained by Fourier transformation from the respective structure factors $a^{\mathrm{Exp-N}}(q)$ and $a^{\mathrm{Exp-X}}(q)$ for the $Bi_{30}Ga_{70}$ liquid alloy at 265 °C.

the sample is evacuated to about 5×10^{-5} mbar and filled with a gas mixture of Ar–10% H_2 (vol%). To assure sample homogenization, the sample is heated up to 700 °C, kept for several hours at this temperature and then cooled slowly down to the experimental temperature.

Mo Kα radiation ($\lambda = 0.711$ Å) diffracted by the free sample surface is selected by a focusing graphite monochromator. The scattered intensity is measured with a scintillation detector with a pulse height analyser. The magnitude of the diffraction vector q ranged from about 0.7 to 12 Å^{-1}. The intensity is recorded in steps of 0.05 Å^{-1} for $q \leqslant 5$ Å^{-1} and in steps of 0.1 Å^{-1} for $q > 5$ Å^{-1}.

The x-ray scattering intensity from liquid $Bi_{30}Ga_{70}$ measured in arbitrary units was converted into the Faber–Ziman structure factor using standard procedures as described in [22].

4. Results and discussion

The experimental FZ total neutron scattering structure factor $a^{\mathrm{Exp-N}}(q)$ and the experimental FZ total x-ray scattering structure factor $a^{\mathrm{Exp-X}}(q)$ for $Bi_{30}Ga_{70}$ liquid alloy at 265 °C are presented in figure 1. Their Fourier transforms $g^{\mathrm{Exp-N}}(r)$ and $g^{\mathrm{Exp-X}}(r)$ are presented in figure 2. For a comparison, the positions of the main peaks on the structure factor and the pair correlation function of pure bismuth at 300 °C [13] and Ga at 200 °C [13] are also shown in figures 1 and 2, respectively.

The experimental structure factors obtained with XRD and ND are significantly different due to the different contribution of Bi and Ga atoms to the total scattering functions. The weight factors w_{ij}^{N} and $w_{ij}^{\mathrm{X}}(q=0)$ for $Bi_{30}Ga_{70}$ composition calculated with equations (2*a*) and (2*b*) are presented in table 1. The contribution of mixed Bi–Ga pairs to the total diffraction curves is rather similar in both XRD and ND experiments. However, the contribution of Bi–Bi pairs to the total structure factor is about 2.5 times larger in the XRD as compared to the ND, while the contribution of Ga–Ga pairs to the XRD total structure factor is approximately half that with the neutron

Table 1. Weight factors for neutron and x-ray scattering. In the case of x-rays the values are calculated for $q = 0$ Å^{-1}.

Atom pair	w_{ij}^{N}	w_{ij}^{X}
Bi–Bi	0.112	0.285
Bi–Ga	0.222	0.249
Ga–Ga	0.444	0.217

diffraction. This is reflected in the shape of the experimental curves plotted in figure 1. The main peak of the XRD structure factor is more intense and shifted to lower q values due to a larger effect of Bi–Bi scattering as compared to ND. A characteristic feature of liquid Bi and Ga is the asymmetry of the first peak on their structure factors. Distinct shoulders on the right-hand side of the first peak are situated at $q = 2.85$ Å^{-1} for liquid Bi and $q = 3.12$ Å^{-1} for liquid Ga as determined by Waseda [13]. This feature is also present on the $a^{\mathrm{Exp-X}}(q)$ and $a^{\mathrm{Exp-N}}(q)$ for liquid $Bi_{30}Ga_{70}$. Due to the different contributions of Bi–Bi and Ga–Ga scattering to the XRD and ND total structure factors, the shoulder at about 2.8 Å^{-1} is stronger on the x-ray curve, while the shoulder at somewhat higher q values is more pronounced on the $a(q)$ obtained with neutron diffraction. Similarly, in figure 2 we see that the main peak of $g^{\mathrm{Exp-X}}(r)$ is closer to that of pure Bi, while the main peak of $g^{\mathrm{Exp-N}}(r)$ is closer to that of pure Ga. The peculiar structure of liquid Bi and Ga as well as the nature of the shoulders on the first peak of their structure factors are beyond the subject of our investigation. These phenomena have been studied, for example, in [23–25].

It has been shown in [19] on the example of Cu_6Sn_5 liquid that reliable partial pair distribution functions and partial structure factors can be obtained with the help of RMC if the experimental XRD and ND total structure factors are modelled simultaneously. Remarkable contrast between the XRD and ND experimental functions for $Bi_{30}Ga_{70}$ liquid (figure 1) enables plausible modelling of its structure in the present study.

The two experimental structure factors $a^{\mathrm{Exp-N}}(q)$ and $a^{\mathrm{Exp-X}}(q)$ and the nearest approach cut-off distances $r_{\mathrm{Bi-Bi}}^{\mathrm{min}} = 3.0$ Å, $r_{\mathrm{Bi-Ga}}^{\mathrm{min}} = 2.7$ Å, $r_{\mathrm{Ga-Ga}}^{\mathrm{min}} = 2.5$ Å are used as input

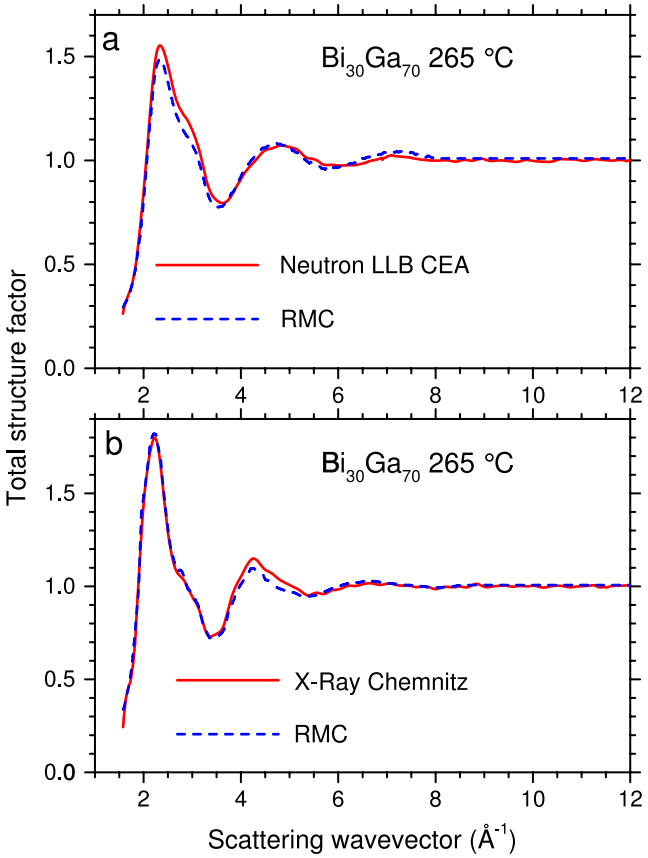

Figure 3. Experimental (*full line*) neutron scattering and x-ray diffraction structure factors for the $Bi_{30}Ga_{70}$ liquid alloy at 265 °C compared to the RMC fits (*dashed line*) obtained by simultaneous simulation of the ND and XRD data.

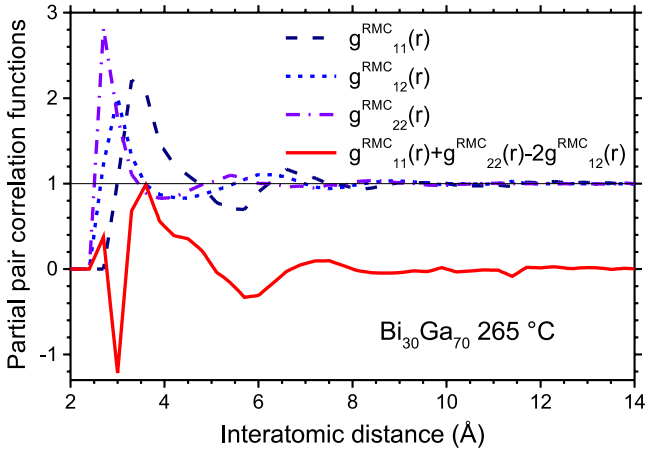

Figure 4. Partial pair correlation functions $g_{ij}^{\mathrm{RMC}}(r)$ for $Bi_{30}Ga_{70}$ liquid alloy at 265 °C obtained with RMC and the linear combination $g_{11}^{\mathrm{RMC}}(r) + g_{22}^{\mathrm{RMC}}(r) - 2g_{12}^{\mathrm{RMC}}(r)$.

Table 2. Structural parameters of $Bi_{30}Ga_{70}$ liquid alloy at 265 °C. r_{ij}^1 are the most probable interatomic distances; N_{ij}^1 are the first coordination numbers.

Coordination	r_{ij}^1 (Å)	N_{ij}^1
Bi–Bi	3.3	4.30
Bi–Ga	3.0	4.61
Ga-Bi	3.0	1.97
Ga–Ga	2.7	5.84

data in the RMC simulations. The alloy number density is estimated to be $\rho_0 = 0.0409$ Å^{-3}, where the mean atomic volume of the alloy is calculated as a linear interpolation of the atomic volumes of pure components [26]. The RMC modelling process has been done with 3000 atoms in a box of 25 Å side length. In figure 3, we compare the XRD and ND experimental structure factors for $Bi_{30}Ga_{70}$ liquid with the RMC fits.

The three pair correlation functions $g_{ij}^{\mathrm{RMC}}(r)$ corresponding to the final atomic configuration obtained with RMC are presented in figure 4 together with the function $g_{11}^{\mathrm{RMC}}(r) + g_{22}^{\mathrm{RMC}}(r) - 2g_{12}^{\mathrm{RMC}}(r)$. It is clearly seen that the Hoshino and Young criterion [8] is checked. Furthermore, the $g_{11}^{\mathrm{RMC}}(r) + g_{22}^{\mathrm{RMC}}(r) - 2g_{12}^{\mathrm{RMC}}(r)$ function is positive in the range 3.2–5.0 Å, which reveals the trend to homo-coordination in the first neighbour shell.

The partial coordination numbers obtained from our pair correlation functions by integration from the left edge of the first peak up to the first minimum are listed in table 2. These numbers allowed us to calculate the Cargill–Spaepen short-range order parameter [11] given by:

$$\eta_{12} = \eta_{21} = \frac{N_{12}^1\langle z\rangle}{c_2 z_1 z_2} - 1, \qquad z_1 = N_{11}^1 + N_{12}^1,$$
$$z_2 = N_{22}^1 + N_{21}^1, \quad \langle z\rangle = c_1 z_1 + c_2 z_2. \tag{7}$$

The resulting value of $\eta_{12} = 0.23$ for $Bi_{30}Ga_{70}$ clearly indicates the preference of homo-coordination.

In figure 5, we compare (i) Bi–Bi partial pair distribution function $g_{11}^{\mathrm{RMC}}(r)$ of liquid $Bi_{30}Ga_{70}$ at 265 °C with the experimental pair distribution function of pure liquid bismuth at 300 °C $g_{\mathrm{Pure\ Bi}}(r)$, (ii) Ga–Ga partial pair distribution function $g_{22}^{\mathrm{RMC}}(r)$ with the experimental pair distribution function of pure liquid gallium at 200 °C and finally (iii) Bi–Ga partial pair distribution function $g_{12}^{\mathrm{RMC}}(r)$ with the half sum $(\frac{g_{\mathrm{Pure\ Bi}}(r)+g_{\mathrm{Pure\ Ga}}(r)}{2})$ of the experimental pair distribution functions for the two pure metals. The crossed pair correlation function $(\frac{g_{\mathrm{Pure\ Bi}}(r)+g_{\mathrm{Pure\ Ga}}(r)}{2})$ corresponds to an alloy with statistical mutual distribution of the two atom types ($S_{\mathrm{CC}}(q) = c_1c_2$ from equations (5) and (6)). In figure 5(a), we see that the main peak of $g_{11}^{\mathrm{RMC}}(r)$ is broader than that of $g_{\mathrm{Pure\ Bi}}(r)$ and that the first minimum of $g_{11}^{\mathrm{RMC}}(r)$ is located at $r = 5.70$ Å, whereas that of $g_{\mathrm{Pure\ Bi}}(r)$ is located at $r = 4.75$ Å. In contrast, we observe in figure 5(b) that the partial pair correlation function $g_{22}^{\mathrm{RMC}}(r)$ and the pair correlation function $g_{\mathrm{Pure\ Ga}}(r)$ have very similar shapes. This indicates that the short-range order around gallium atoms in the liquid $Bi_{30}Ga_{70}$ alloy is very close to that in pure liquid gallium. In figure 5(c), the main peak of $g_{12}^{\mathrm{RMC}}(r)$ is located at $r = 3.00$ Å whereas that of $(\frac{g_{\mathrm{Pure\ Bi}}(r)+g_{\mathrm{Pure\ Ga}}(r)}{2})$ is located at $r = 3.30$ Å which leads to a reduction of in the number of the different species' neighbours because the minima of the two pair correlation functions are located at the same position $r = 4.40$ Å. On the other hand, the atomic arrangement around bismuth atoms in the liquid $Bi_{30}Ga_{70}$ differs from that in liquid bismuth. These findings are similar to those obtained by Saito *et al* [10].

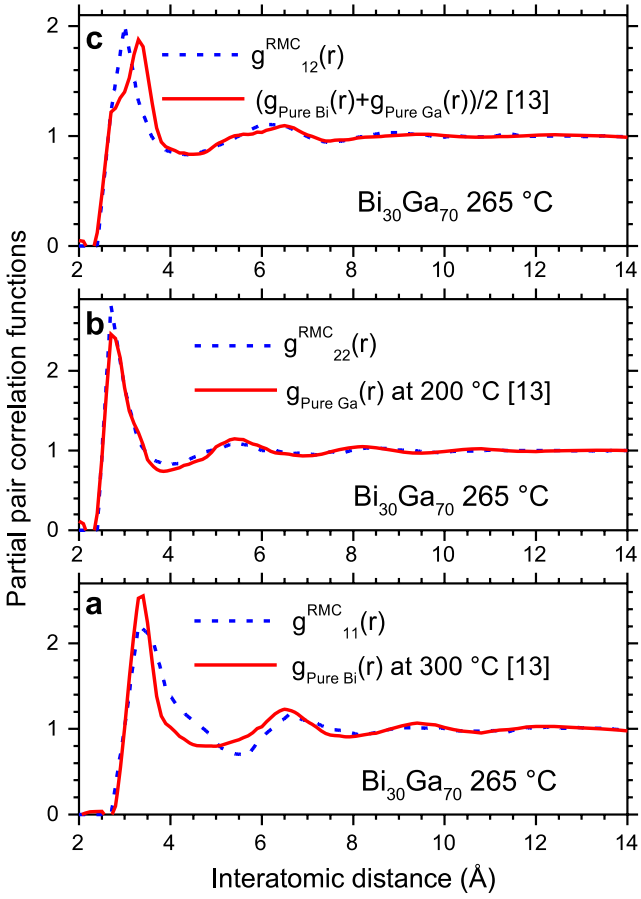

Figure 5. Comparison of the three modelled partial pair correlation functions $g_{ij}^{\mathrm{RMC}}(r)$ (*dashed lines*) with the pure metal experimental pair correlation functions (*full lines*) [13]. (a) for Bi–Bi pairs and pure Bi, (b) for Ga–Ga pairs and pure Ga, (c) for Bi–Ga pairs and $(\frac{g_{\mathrm{Pure\ Bi}}(r)+g_{\mathrm{Pure\ Ga}}(r)}{2})$ function.

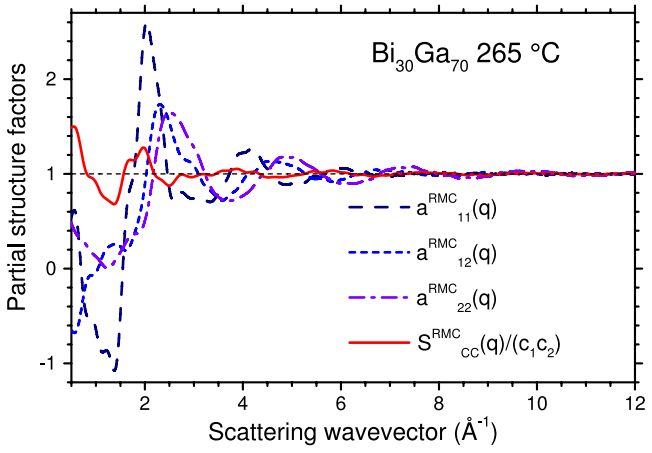

Figure 6. Partial structure factors $a_{ij}^{\mathrm{RMC}}(q)$ obtained from the modelled $g_{ij}^{\mathrm{RMC}}(r)$ by Fourier transform and reduced Bhatia–Thornton partial structure factor $S_{\mathrm{CC}}^{\mathrm{RMC}}(q)/(c_1c_2)$ for $Bi_{30}Ga_{70}$ liquid alloy at 265 °C.

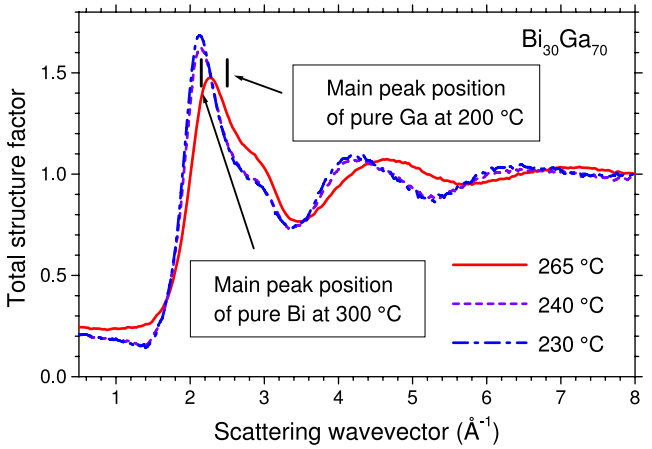

Figure 7. $Bi_{30}Ga_{70}$ total structure factors $a^{\mathrm{N}}(q)$ obtained from neutron scattering above the critical temperature at 265 °C and below the critical temperature at 240 and 230 °C.

The results can be explained if the Bi–Ga phase diagram is considered. The composition of Ga-rich liquid at the monotectic temperature is $Bi_{8.5}Ga_{91.5}$, while the composition of Bi-rich liquid is $Bi_{61.5}Ga_{38.5}$ [9]. This means that in the case of micro-segregation near the critical temperature, the local order around Ga atoms can be expected to be closer to that in the liquid $Bi_{8.5}Ga_{91.5}$ alloy or pure gallium, while the short-range ordering around Bi atoms should be closer to that in the liquid $Bi_{61.5}Ga_{38.5}$ rather than that in pure liquid bismuth.

The trend to homo-coordination is also checked in reciprocal space by analysis of the partial structure factors $a_{ij}^{\mathrm{RMC}}(q)$ calculated with equation (4). They are displayed along with the reduced Bhatia–Thornton partial structure factor $S_{\mathrm{CC}}^{\mathrm{RMC}}(q)/(c_1c_2)$ in figure 6. This figure shows clearly the increasing of the $a_{11}^{\mathrm{RMC}}(q)$ and $a_{22}^{\mathrm{RMC}}(q)$ and the decreasing of $a_{12}^{\mathrm{RMC}}(q)$ for q between 0.4 and 1.4 Å^{-1}. The increase of $S_{\mathrm{CC}}(q)/(c_1c_2)$ is also seen at the same q range. The criteria of segregation cannot be obtained for $q < 0.5$ Å^{-1} because of limited size of the RMC simulation box: $q_{\min} = 2\pi/(L/2) = 0.50$ Å^{-1}, where $L = 25$ Å is the side length.

Finally, we present the results of temperature effects on the structure of $Bi_{30}Ga_{70}$ liquid alloy. Figure 7 exhibits the structure factors of liquid $Bi_{30}Ga_{70}$ measured in the lower part of the sample, at a temperature of 265 °C, which is slightly above the critical temperature $T_{\mathrm{C}} = 262$ °C and at temperatures of 240 and 230 °C, i.e. below T_{C}. For a comparison, the positions of the main peaks on the experimental structure factors of pure liquid Bi and Ga are shown [13]. It appears clearly that when we reach the segregation region in the phase diagram, then there is a remarkable displacement of the main peak of the $Bi_{30}Ga_{70}$ structure factor towards that of pure bismuth, which indicates an increasing bismuth concentration in the lower part of the sample when the temperature decreases. The same behaviour is observed on the corresponding pair correlation functions presented in figure 8 together with the positions [13] of the main peaks of the pure metal pair correlation functions. The position of the first peak on the $g(r)$ for the liquid $Bi_{30}Ga_{70}$ does not coincide with that of pure bismuth because the Bi-rich liquid still contains at least 38.5 at.% Ga [9].

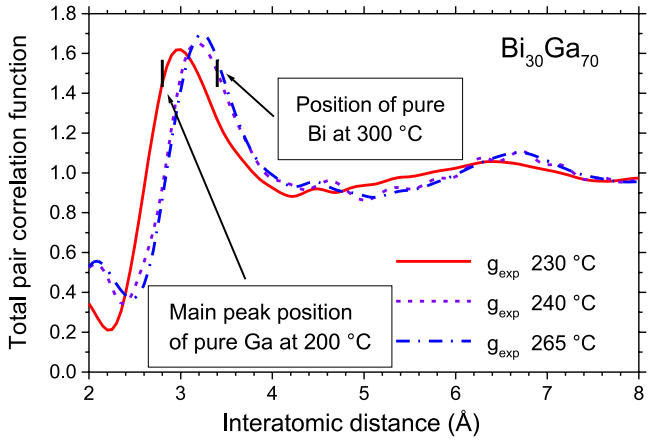

Figure 8. $Bi_{30}Ga_{70}$ total pair correlation function $g^{N}(r)$ above the critical temperature at 265 °C and below the critical temperature at 240 and 230 °C.

5. Conclusion

By analysis of the two independent scattering experiments and RMC modelled structure of liquid $Bi_{30}Ga_{70}$, we showed that atomic segregation in the alloy of critical concentration starts to develop in the single-phase liquid by approaching the critical point. This is manifested by the partial structure functions on the real space scale as well as in the reciprocal space. Various criteria of the segregation are fulfilled; in particular the negative Cargill–Spaepen short-range order parameter gives quantitative proof of homo-coordination. The short-range order around gallium atoms in the $Bi_{30}Ga_{70}$ alloy near the critical temperature is similar to that of pure liquid Ga. The atomic arrangement around bismuth atoms in liquid $Bi_{30}Ga_{70}$ is suggested to be closer to that in liquid $Bi_{61.5}Ga_{38.5}$ than in pure bismuth. These similarities become more evident from the consideration of the structure of the Bi-rich separated phase in the liquid $Bi_{30}Ga_{70}$ alloy below the critical temperature.

References

[1] Singh R N and Sommer F 1997 *Rep. Prog. Phys.* **60** 57
[2] Inui M and Takeda S 1993 *J. Non-Cryst. Solids* **156–158** 153
[3] Ginter G, Gasser J G and Kleim R 1986 *Phil. Mag.* B **54** 543
[4] Vollmann J and Riedel D 1996 *J. Phys.: Condens. Matter* **8** 6175
[5] Wignall G D and Egelstaff P A 1968 *J. Phys. C: Solid State Phys.* **1** 1088
[6] Halm Th, Nomssi Nzali J, Hoyer W and May R P 1999 *J. Non-Cryst. Solids* **250–252** 293
[7] Bhatia A B and Thornton D E 1970 *Phys. Rev.* B **2** 3004
[8] Hoshino K and Young W H 1986 *J. Phys. F: Met. Phys.* **16** 1671
[9] Massalski T B, Murray J L, Bennet K H and Baker H 1986 *Binary Alloy Phase Diagrams* vol 1 (Metals Park, OH: American Society for Metals)
[10] Saito M, Park C, Sugiyama K and Waseda Y 1997 *J. Phys. Soc. Japan* **66** 3120
[11] Cargill G S and Spaepen F 1981 *J. Non-Cryst. Solids* **43** 91
[12] Faber T E 1972 *An Introduction to the Theory of Liquid Metals* (London: Cambridge University Press)
[13] Waseda Y 1980 *The Structure of Non-Crystalline Materials* (New York: McGraw-Hill)
[14] Koester L and Yelon W B 1982 *Summary of Low Energy Neutron Scattering Lengths and Cross Sections* Netherlands Research Foundation
[15] Ruppersberg H and Knoll W 1977 *Z. Naturf.* a **32** 1374
[16] McGreevy R L and Pusztai L 1988 *Mol. Simul.* **1** 359
[17] McGreevy R L and Pusztai L 2001 *J. Phys.: Condens. Matter* **13** R877
[18] Gruner S, Akinlade O and Hoyer W 2006 *J. Phys.: Condens. Matter* **18** 4773
[19] Kaban I, Gruner S, Hoyer W, Jóvári P, Delaplane R G and Wannberg A 2007 *J. Non-Cryst. Solids* **353** 3027
[20] Ambroise J P, Bellissent-Funel M C and Bellissent R 1984 *Rev. Phys. Appl.* **19** 731
[21] Paalmam H H and Pings C J 1962 *J. Appl. Phys.* **33** 2635
Blech I A and Averbach B L 1965 *Phys. Rev.* A **137** 1113
Placzek G 1952 *Phys. Rev.* **86** 377
Yarnell J L *et al* 1973 *Phys. Rev.* A **7** 2130
[22] Kaban I, Hoyer W, Il'inskii A, Slukhovskii O and Slyusarenko S 2003 *J. Non-Cryst. Solids* **331** 254
[23] Zhou X-W, Jin Z-Z and Shang Y-J 1987 *Phys. Status Solidi* b **139** 365
[24] Tsay S-F and Wang S 1994 *Phys. Rev.* B **50** 108
[25] Tsai K H, Wu T-M, Tsay S-F and Yang T-J 2007 *J. Phys.: Condens. Matter* **19** 205141
[26] Crawley A F 1974 *Int. Met. Rev.* **19** 32